Kristofer Leach (Autor)

Modelling Force Transfer in Boundary Layers of Moving Walls for Compressible and Incompressible Turbulent Flows Across Multiple Scales

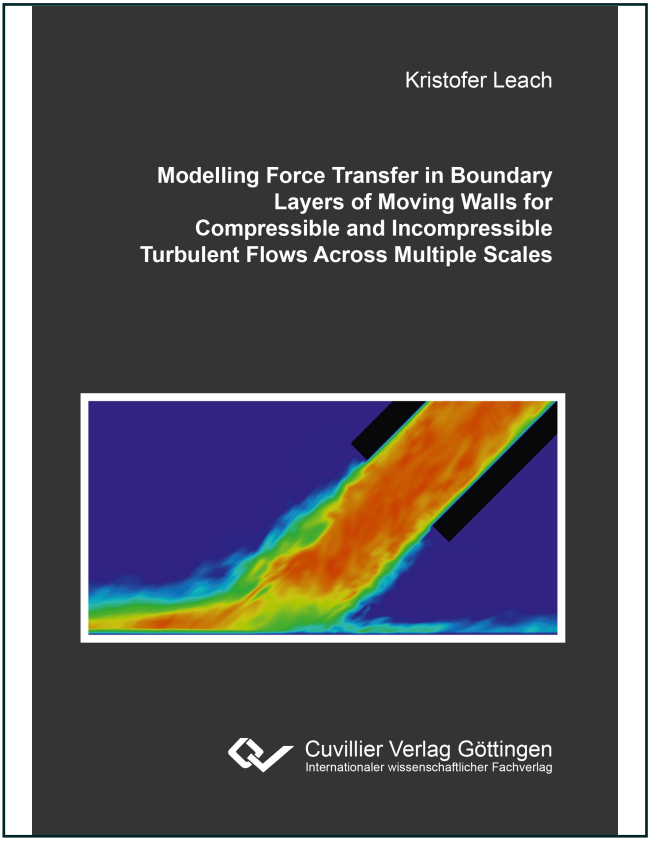

https://cuvillier.de/de/shop/publications/6886

Chapter 1

Introduction

Project *GrindBall* is an applied research project sponsored by the German Research Foundation (DFG) as part of the work-group *Small Machine Tools* (SPP 1476) involving simulation, electro-magnetic control, and manufacture of a miniature abrading device. The workload in this project is hence distributed across three institutes: computational simulation is conducted at the *Center of Applied Space Technology and Microgravity* (ZARM), the electro-magnetic control element is developed at the *Institute for Electrical Drives, Power Electronics and Devices* (IALB), and manufacture of the tool itself is undertaken by the *Laboratory for Precision Machining* (LFM).

1.1 Motivation

Miniaturisation is of great importance in many fields such as mechantronics, optics, or medicine as it enables new functionality or makes processes more economical [BRB+13]. Micro-grinding, for example, can be performed with extremely high precision. While this increasing precision [DMT06] has made it possible to produce smaller and smaller workpieces, the tools used to work on them have, for the most part, remained constant in size [WRK10]. The skewed ratio of tool size to workpiece size is creating a growing ecological, economic, and technical inefficiency regarding respective processes [WGKK12]. Until now, miniaturising existing tools has been performed in order to combat said skewed ratio. This approach is, however, reaching its limits regarding technical feasibility and usefulness [ASB10]. For this reason, new innovative concepts and tools need to be developed, which are specifically designed to cope with small workpieces and spatially confined environments, in order to make progress in production processes such as micro-machining and ultra precise machining. It has already been shown that new operating principles and technologies present innovative methods of miniaturisation that supersede a mere reduction in size of pre-existing tools [BRB+13, DMK12]. This field possesses a lot of potential in terms of research and development of new tools which will be capable of outperforming currently available technologies. Workspace utilisation and energy requirements can still be vastly improved upon. Furthermore, the tools' susceptib-

ility to thermal deformation effects can be greatly reduced as a result of their smaller size [BRB+13]. Further direct results of miniature tools are increased flexibility and design possibilities concerning the machining of small workpieces since micro-tools can quickly adapt to new production procedures.

Since the ratio of surface area to volume increases dramatically with increasing miniaturisation, one has, proportionally, far more functional surface to work with as volume decreases. This effect is extremely useful for abrasive tools because the control dynamics, for example, improve with decreasing tool size, thus also improving the tools ability to adapt to particular machining conditions [BRB+13]. Most abrasive tools used to create micro cavities suffer from the following problem: since the axis of rotation and its orientation to the workpiece are crucial in ensuring positive grinding results, aligning the axis of rotation is key when grinding a cavity. A grinding pencil, for instance, has its theoretical maximum effectiveness when the axis of rotation is parallel to the work piece. This, however, can often be difficult to achieve as the grinding pencil's mounting apparatus can touch down on to the work piece before maximum effectiveness can be reached. Also, should the axis of rotation be perpendicular to the workpiece, the grinding pencil's abrasion would tend to zero. This problem can be counteracted by tilting the apparatus slightly, however, this still delivers mediocre results because it does not maximise the tool's effectiveness. Figure 1.1 illustrates the problems stated along with a theoretical solution in which the axis of rotation is parallel to the workpiece at all times, thus maximising the tool's grinding efficiency. It is the goal of project *GrindBall* to develop a spherical grinding tool, which, in addition, combines propulsion and control into one single element. The intended result is a highly compact, precise, efficient, and adaptive miniature tool, which can be used as a desktop machine for processing non-magnetic workpieces such as glass or ceramic. Possible applications include manufacturing dentures or miniature camera lenses as are used in modern smart phones (which require extreme precision) to name just a few.

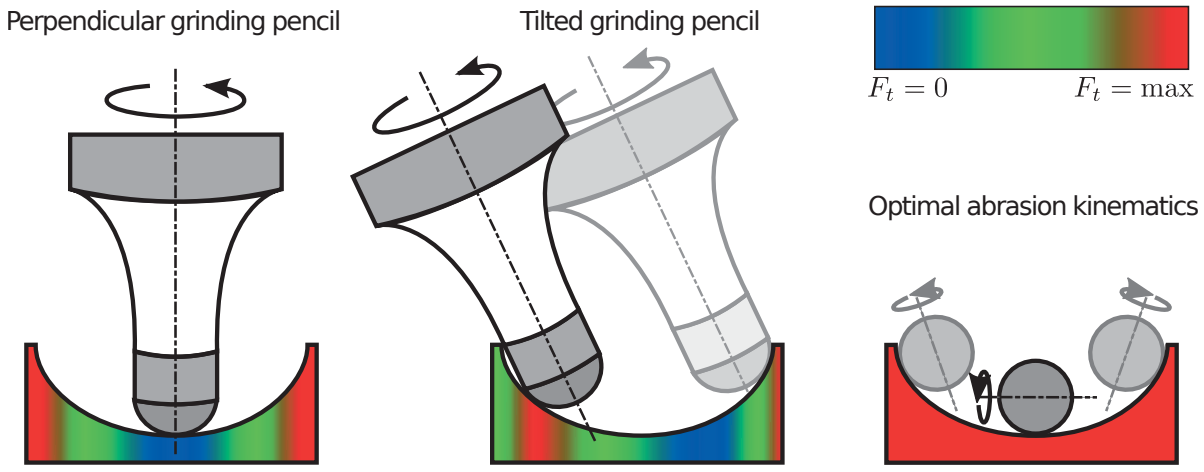

Figure 1.1: Grinding force depending on axis orientation

1.2 Basic setup

To achieve development of such a tool, fluid-driven propulsion is used in conjunction with a ferromagnetic sphere which is either covered in an abrasive coating or made entirely of abrasive material. It has already been shown that a variety of new production processes can achieve pleasing results concerning the manufacture of viable grinding spheres [BGB12, BRKB13]. In particular, injection moulding of micro-particle filled polymers has been shown to perform well in experiments conducted by the LFM and presents a viable option for use with the *GrindBall* [BRKB13].

Displacing forces are to be compensated by an adjustable opposing force, so that the sphere is held in a predefined position relative to the shaft at all times (as seen in Figure 1.2). Such displacing forces include gravity, vibration, forces resulting from the process of machining workpieces, and of course forces exerted by the fluid propulsion, all of which are to be counteracted. This task is performed by a magnetic bearing, which in addition to controlling the position of the grinding sphere, also defines an axis of rotation in combination with the flow. Experiments and simulations conducted by the IALB have shown that this concept can prove to meet the requirements demanded by this project and mathematical models were derived which aid in magnetically controlling and adjusting the position of the grinding sphere relative to the grinding shaft [Nor12, BOG+13].

The first prototype will utilise a sphere with a diameter of 40 mm. Throughout the duration of project *GrindBall*, this diameter is to be gradually scaled down to 1 mm with surrounding elements shrinking in proportion. The force necessary to achieve abrasion will be applied by the fluid flow. Due to the sphere having little mass and the resulting low moment of inertia, rotational frequencies in excess of 10,000 rpm and an extremely high control dynamic and accuracy are to be expected. Planning and construction of the *GrindBall* requires interdisciplinary cooperation between three branches of production technology: manufacturing engineering, electrical engineering, and fluid mechanics.

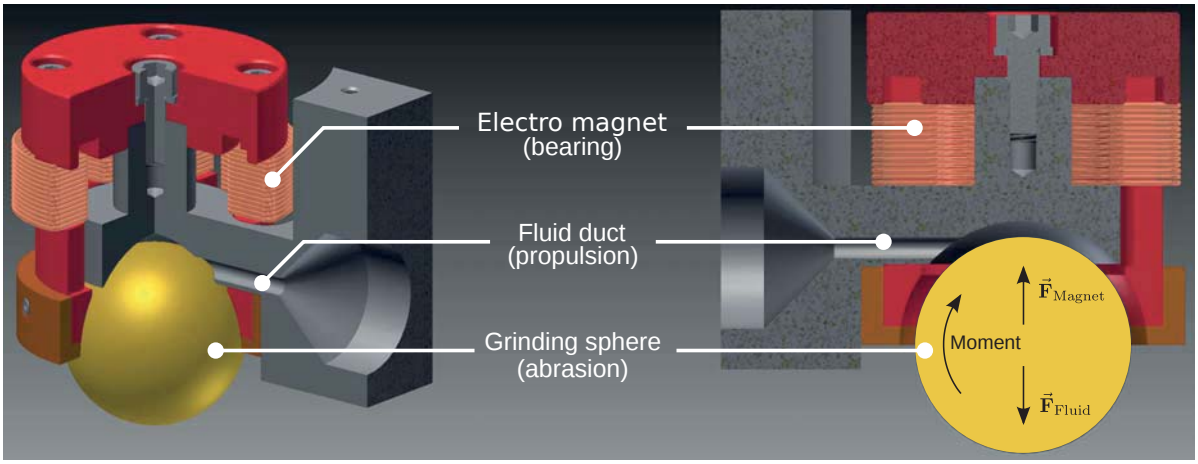

Figure 1.2: *GrindBall* - basic setup

1.3 Goals and limitations

This thesis begins by introducing the knowledge necessary to conduct computational simulations in the scope of this project, i.e. by deriving the equations governing fluid flow and stating common computational methods used in CFD simulations. Focus is drawn to the Finite Volume Method (FVM) and the modelling of turbulence using Large Eddy Simulation (LES). Throughout, the discussion is limited to sub-sonic flow and the use of adiabatic walls with uniform initial temperature distribution. Supersonic flow, heat-transferring walls, and temperature gradients on walls are best discussed once actual grinding trails have been performed and more data is available regarding the magnetic bearing's capabilities, material properties, and production of heat both by the bearing and the grinding process.

A parametric study is performed to determine the optimal configuration of a prototype tool with a 40 mm sphere using pneumatic propulsion (air). Once found, the optimal layout is subjected to a multitude of simulations under varying volumetric flow rates and spherical rotation frequencies, which ascertain the *GrindBall*'s possibilities and limitations. This includes identifying conditions for stable and efficient operation of the tool, quantifying acting forces, and deriving mathematical models which govern the force and power available to the abrasion process.

A fully functional version of the tool is devised with a spherical diameter of 8 mm using the knowledge gained from the development of the prototype. Parametric studies determine an optimal propulsion fluid and further improve the geometric layout. Forces and power are determined and discussed.

Simulation results - with specific focus on forces exerted by fluid impacting on to solid bodies - are validated by devising and performing an experiment with which to empirically confirm the presented findings. This is done using a setup consistent with the developed prototype. However, moving walls, which are analogous to a rotating grinding sphere, can not considered in the experimental setup.

Finally, a study is carried out using pneumatic propulsion which determines both forces and power for three different spherical diameters. These cover laminar, transitional, and fully turbulent flow. Using the resulting findings, non-dimensional relations are derived which govern forces and power depending on Reynolds number and a dimesionless spherical rotation frequency. Not only are the differences between laminar and turbulent flow made apparent, the need for further simulations with this geometry is eliminated as the resulting relations can be applied to arbitrary scales. Furthermore, it is shown that this type of analysis can be used both to compare different propulsion media and varying geometric layouts.

Knowledge of grinding force and power is extremely important when machining workpieces as it ensures that the rotation frequency and the cutting speed can be adapted

to particular materials, thereby ensuring accurate manufacturing of high quality cavities with smooth surfaces. The analyses conducted within this thesis pave the way for the development of a novel and revolutionary new grinding tool and demonstrate how fluid-to-solid force transfer can be modelled across a multitude of scales.

Chapter 2

Governing equations

The following section derives the equations which govern the flow of Newtonian compressible fluids and gives an overview of the concepts behind their derivations. Their incompressible equivalents are stated and specific models such as the perfect gas law and Sutherland's viscosity model are introduced.

2.1 Conservation of mass

Let ψ denote an arbitrary intensive property defined over a material control volume V. The Reynolds transport theorem[1] states that the rate of change of ψ within V must be equal to the sum of the flux of ψ over the volume boundaries δV and sources or sinks Q within V:

$$\frac{\mathrm{d}}{\mathrm{d}t}\int_V \psi \,\mathrm{d}V = -\int_{\delta V} \psi \underline{\mathbf{u}} \cdot \underline{\mathbf{n}} \,\mathrm{d}A + \int_V Q \,\mathrm{d}V. \tag{2.1}$$

Using the divergence theorem[1], the surface integral becomes a volume integral:

$$\frac{\mathrm{d}}{\mathrm{d}t}\int_V \psi \,\mathrm{d}V = -\int_V \nabla \cdot (\psi \underline{\mathbf{u}}) \,\mathrm{d}V + \int_V Q \,\mathrm{d}V. \tag{2.2}$$

Also the LHS can be written as

$$\frac{\mathrm{d}}{\mathrm{d}t}\int_V \psi \,\mathrm{d}V = \int_V \frac{\partial \psi}{\partial t} \,\mathrm{d}V \tag{2.3}$$

using Leibniz's integral rule[1]. Now the volume integrals may be combined into one single integral:

$$\int_V \frac{\partial \psi}{\partial t} + \nabla \cdot (\psi \underline{\mathbf{u}}) - Q \,\mathrm{d}V = 0. \tag{2.4}$$

[1] See Appendix A

Since this must hold for an arbitrary volume V, the integrand itself must equal zero. Hence,

$$\frac{\partial \psi}{\partial t} + \nabla \cdot (\psi \underline{\mathbf{u}}) - Q = 0. \tag{2.5}$$

This generic equation of continuity (eqn (2.5)) may be used to derive various conservation laws. The most basic such law is obtained by substituting the mass density ρ for ψ and assuming $Q = 0$, i.e. mass is neither created nor destroyed:

$$\frac{\partial \rho}{\partial t} + \nabla \cdot (\rho \underline{\mathbf{u}}) = 0. \tag{2.6}$$

This is known as the *mass continuity equation*, often also simply referred to as *the continuity equation* (cp. [Whi05]).

2.2 Conservation of momentum

In a similar yet somewhat less straight forward way, $\rho\underline{\mathbf{u}}$ may be substituted into eqn (2.5) to derive a relation for the rate of change of momentum. Note that Q is replaced by $\underline{\mathbf{f}}$, a vector representing sources and sinks of momentum, i.e. forces per unit volume:

$$\frac{\partial (\rho \underline{\mathbf{u}})}{\partial t} + \nabla \cdot (\rho \underline{\mathbf{u}} \otimes \underline{\mathbf{u}}) - \underline{\mathbf{f}} = 0. \tag{2.7}$$

Expanding the derivatives once yields

$$\frac{\partial \rho}{\partial t}\underline{\mathbf{u}} + \rho \frac{\partial \underline{\mathbf{u}}}{\partial t} + \nabla (\rho \underline{\mathbf{u}}) \cdot \underline{\mathbf{u}} + \rho \underline{\mathbf{u}} \nabla \cdot \underline{\mathbf{u}} = \underline{\mathbf{f}}, \tag{2.8}$$

which can be further decomposed into

$$\frac{\partial \rho}{\partial t}\underline{\mathbf{u}} + \rho \frac{\partial \underline{\mathbf{u}}}{\partial t} + \nabla (\rho)\, \underline{\mathbf{u}} \cdot \underline{\mathbf{u}} + \rho \nabla (\underline{\mathbf{u}}) \cdot \underline{\mathbf{u}} + \rho \underline{\mathbf{u}} \nabla \cdot \underline{\mathbf{u}} = \underline{\mathbf{f}}. \tag{2.9}$$

The following rearrangement highlights common factors ρ and $\underline{\mathbf{u}}$:

$$\underline{\mathbf{u}} \frac{\partial \rho}{\partial t} + \rho \frac{\partial \underline{\mathbf{u}}}{\partial t} + \underline{\mathbf{u}}\underline{\mathbf{u}} \cdot \nabla \rho + \rho \underline{\mathbf{u}} \cdot \nabla \underline{\mathbf{u}} + \rho \underline{\mathbf{u}} \nabla \cdot \underline{\mathbf{u}} = \underline{\mathbf{f}}, \tag{2.10}$$

which may be collected thusly:

$$\rho \left(\frac{\partial \underline{\mathbf{u}}}{\partial t} + \underline{\mathbf{u}} \cdot \nabla \underline{\mathbf{u}} \right) + \underline{\mathbf{u}} \left(\frac{\partial \rho}{\partial t} + \underline{\mathbf{u}} \cdot \nabla \rho + \rho \nabla \cdot \underline{\mathbf{u}} \right) = \underline{\mathbf{f}}. \tag{2.11}$$

At this point it is worth noting that the expression inside the second parenthesis on the LHS of eqn (2.11) is equal to the LHS of eqn (2.6), which is equal to zero. Hence, conservation of momentum is given by

$$\rho \frac{\partial \underline{\mathbf{u}}}{\partial t} + \rho \underline{\mathbf{u}} \cdot \nabla \underline{\mathbf{u}} = \underline{\mathbf{f}}. \tag{2.12}$$

$\underline{\mathbf{f}}$ is typically further divided into surface forces and body forces. Body forces are those which apply to the entire mass of the control volume. Such forces are usually gravitational or electromagnetic in nature. Here only gravity is considered, and thus

$$\underline{\mathbf{f}} = \underline{\mathbf{f}}_{\text{body}} + \underline{\mathbf{f}}_{\text{surface}} = \rho\underline{\mathbf{g}} + \underline{\mathbf{f}}_{\text{surface}}, \tag{2.13}$$

where $\underline{\mathbf{g}}$ is the vector acceleration of gravity.

Surface forces describe forces applied by external stresses on the sides of the volume element. These stresses consist of 9 components and are described by the tensor

$$\underline{\underline{\boldsymbol{\sigma}}} = \begin{pmatrix} \sigma_{xx} & \sigma_{xy} & \sigma_{xz} \\ \sigma_{yx} & \sigma_{yy} & \sigma_{yz} \\ \sigma_{zx} & \sigma_{zy} & \sigma_{zz} \end{pmatrix}. \tag{2.14}$$

$\underline{\underline{\boldsymbol{\sigma}}}$ is a symmetric tensor, i.e. $\sigma_{ij} = \sigma_{ji}$. Symmetry is required to satisfy equilibrium of moments about the three axes of the volume element and will be discussed in section 2.4. Note that the entries in the ith row of $\underline{\underline{\boldsymbol{\sigma}}}$ correspond to the forces acting on the surface facing in the direction of i. Entries in the jth column correspond to forces that act in the direction of j. Figure 2.1 shows individual components σ_{ij} acting on a control volume. Hence, the total force in each direction exerted by stress is given by

$$\begin{aligned} \mathrm{d}F_x &= \sigma_{xx}\mathrm{d}y\mathrm{d}z + \sigma_{yx}\mathrm{d}x\mathrm{d}z + \sigma_{zx}\mathrm{d}x\mathrm{d}y \\ \mathrm{d}F_y &= \sigma_{xy}\mathrm{d}y\mathrm{d}z + \sigma_{yy}\mathrm{d}x\mathrm{d}z + \sigma_{zy}\mathrm{d}x\mathrm{d}y \\ \mathrm{d}F_z &= \sigma_{xz}\mathrm{d}y\mathrm{d}z + \sigma_{yz}\mathrm{d}x\mathrm{d}z + \sigma_{zz}\mathrm{d}x\mathrm{d}y. \end{aligned}$$

In equilibrium, these forces would be balanced by equal and opposite forces on the back faces of the volume. However, if the element were to accelerate, stresses on the front and back would differ by differential amounts. In the direction of x, for example,

$$\sigma_{xx,\text{front}} = \sigma_{xx,\text{back}} + \frac{\partial\sigma_{xx}}{\partial x}\mathrm{d}x, \tag{2.15}$$

resulting in a net force on the volume element in the direction of x:

$$\mathrm{d}F_{x,\text{net}} = \left(\frac{\partial\sigma_{xx}}{\partial x}\mathrm{d}x\right)\mathrm{d}y\mathrm{d}z + \left(\frac{\partial\sigma_{yx}}{\partial y}\mathrm{d}y\right)\mathrm{d}x\mathrm{d}z + \left(\frac{\partial\sigma_{zx}}{\partial z}\mathrm{d}z\right)\mathrm{d}x\mathrm{d}y. \tag{2.16}$$

Or, dividing by $V = \mathrm{d}x\mathrm{d}y\mathrm{d}z$ and taking into account the symmetry of $\underline{\underline{\boldsymbol{\sigma}}}$:

$$f_x = \frac{\partial\sigma_{xx}}{\partial x} + \frac{\partial\sigma_{xy}}{\partial y} + \frac{\partial\sigma_{xz}}{\partial z}, \tag{2.17}$$

which is equivalent to taking the divergence of the vector composed of the top row of the stress tensor. Similarly, f_2 and f_3 are the divergences of the second and third row of $\underline{\underline{\boldsymbol{\sigma}}}$ respectively. Thus, the total vector surface force is

$$\underline{\mathbf{f}}_{\text{surface}} = \nabla\cdot\underline{\underline{\boldsymbol{\sigma}}} = \frac{\partial\sigma_{ij}}{\partial x_j}, \tag{2.18}$$

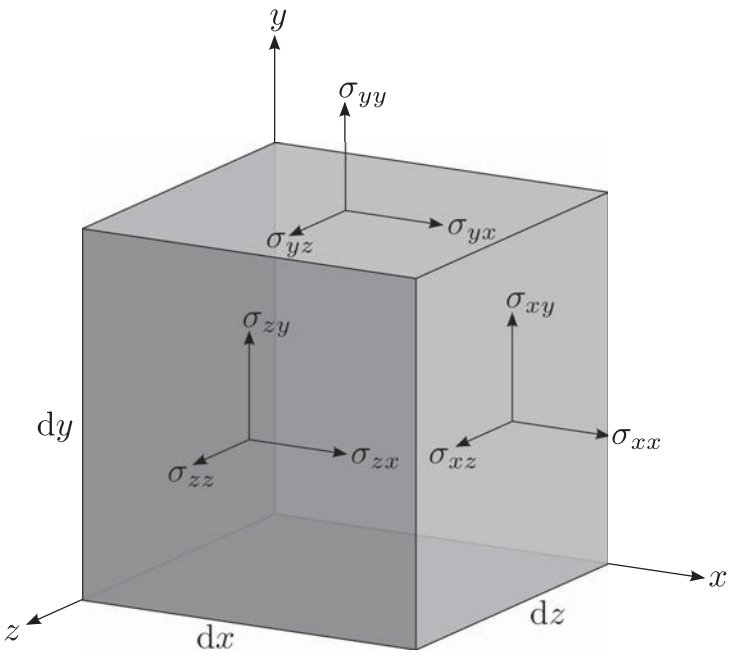

Figure 2.1: Stresses σ_{ij} acting on a control volume

where $\nabla \cdot \underline{\underline{\boldsymbol{\sigma}}}$ is to be interpreted in the tensor sense, resulting in a vector. Eqn (2.12) now becomes

$$\rho \frac{\partial \underline{\mathbf{u}}}{\partial t} + \rho \underline{\mathbf{u}} \cdot \nabla \underline{\mathbf{u}} = \nabla \cdot \underline{\underline{\boldsymbol{\sigma}}} + \rho \underline{\mathbf{g}} \tag{2.19}$$

and it remains to express $\underline{\underline{\boldsymbol{\sigma}}}$ in terms of the velocity $\underline{\mathbf{u}}$. In order to do this, the type of fluid must be taken into consideration. Here, only *Newtonian fluids* are examined, i.e. fluids in which stress is considered a linear function of rate of strain.

2.3 Motion and deformation of a fluid element

In fluid mechanics it is important to be able to describe and quantify motion, deformation, and rate of deformation of fluid elements. Four different types of motion and deformation typically exist: *translation*, *rotation*, *extensional strain* (*dilatation*), and *shear strain*. A 2D example of these four types can be seen in Figure 2.2. Point B is subject to translation as it has moved to the new position B'. The diagonal $\overline{BD}$ represented by the dashed line has been slightly rotated counter-clockwise to $\overline{B'D'}$. Dilatation can be seen in that the element has gained in size. Finally, the element has been subjected to shear strain as it is no longer square but now possesses a rhombic shape.

Now for a more analytical approach. Translation is defined using the displacements of the point B, namely $u\mathrm{d}t$ and $v\mathrm{d}t$. Hence, the rate of translation is simply u and v.

The rotation of $\overline{BD}$ is given by $\mathrm{d}\Omega_z = \theta + \mathrm{d}\alpha - \frac{\pi}{4}$. Noting the fact that $2\theta + \mathrm{d}\alpha + \mathrm{d}\beta = \frac{\pi}{2}$,

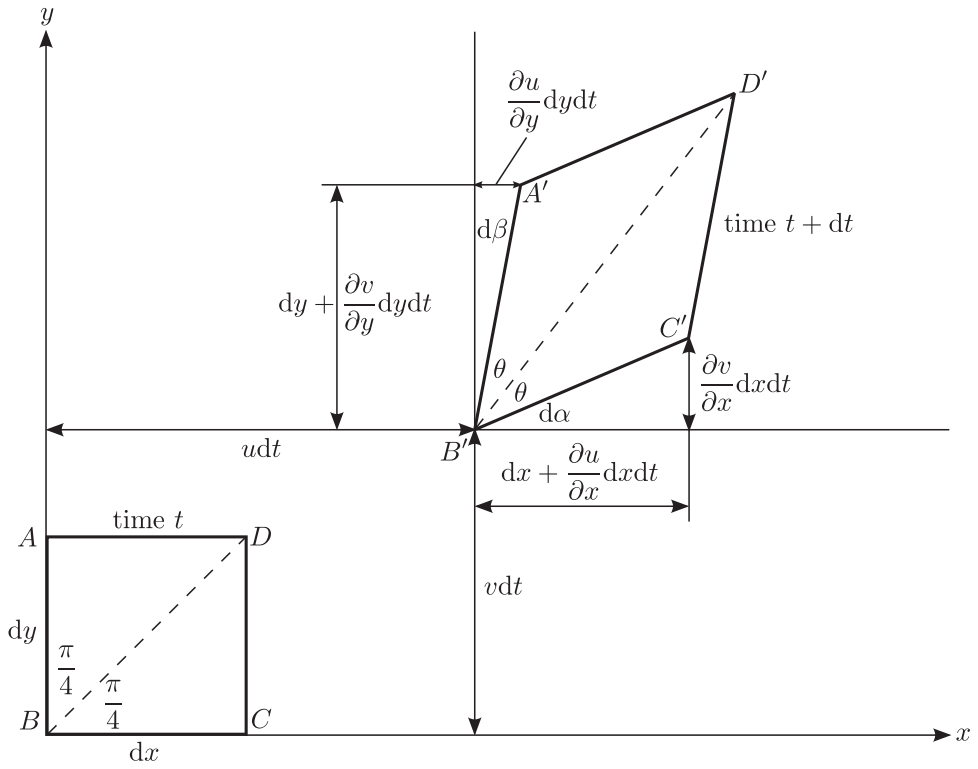

Figure 2.2: Distortion of a moving fluid element (as seen in [Whi05])

θ may be eliminated from the previous expression, leaving

$$\mathrm{d}\Omega_z = \frac{1}{2}\left(\mathrm{d}\alpha - \mathrm{d}\beta\right). \tag{2.20}$$

Both $\mathrm{d}\alpha$ and $\mathrm{d}\beta$ are linked to derivatives of velocity by

$$\begin{aligned}
\mathrm{d}\alpha &= \lim_{\mathrm{d}t\to 0}\left(\tan^{-1}\frac{\frac{\partial v}{\partial x}\mathrm{d}x}{\mathrm{d}x+\frac{\partial u}{\partial x}\mathrm{d}x\mathrm{d}t}\right)\mathrm{d}t = \frac{\partial v}{\partial x}\mathrm{d}t \\
\mathrm{d}\beta &= \lim_{\mathrm{d}t\to 0}\left(\tan^{-1}\frac{\frac{\partial u}{\partial y}\mathrm{d}y}{\mathrm{d}y+\frac{\partial v}{\partial y}\mathrm{d}y\mathrm{d}t}\right)\mathrm{d}t = \frac{\partial u}{\partial y}\mathrm{d}t,
\end{aligned} \tag{2.21}$$

which is valid for small angles. Eqn (2.21) may be substituted into (2.20) to yield the rate of rotation (also referred to as the *angular velocity)* about the z-axis:

$$\frac{\mathrm{d}\Omega_z}{\mathrm{d}t} = \frac{1}{2}\left(\frac{\partial v}{\partial x} - \frac{\partial u}{\partial y}\right). \tag{2.22}$$

Similarly, now for a 3D flow, the rates of rotation about the x and y axis are

$$\frac{\mathrm{d}\Omega_x}{\mathrm{d}t} = \frac{1}{2}\left(\frac{\partial w}{\partial y} - \frac{\partial v}{\partial z}\right) \qquad \frac{\mathrm{d}\Omega_y}{\mathrm{d}t} = \frac{1}{2}\left(\frac{\partial u}{\partial z} - \frac{\partial w}{\partial x}\right). \tag{2.23}$$

Since there is a factor $\frac{1}{2}$ in each of these 3 terms, the *vorticity* $\underline{\boldsymbol{\omega}}$ usually takes preference over $\frac{\mathrm{d}\underline{\boldsymbol{\Omega}}}{\mathrm{d}t}$, as it is equal to twice the angular velocity:

$$\underline{\boldsymbol{\omega}} = 2\frac{\mathrm{d}\underline{\boldsymbol{\Omega}}}{\mathrm{d}t} \tag{2.24}$$

Closer inspection of eqn (2.22) to eqn (2.24) shows their relation through vector calculus:

$$\underline{\boldsymbol{\omega}} = \nabla \times \underline{\mathbf{u}} \tag{2.25}$$

Hence, the vorticity is identically divergence free (or solenoidal):

$$\nabla \cdot \underline{\boldsymbol{\omega}} = \nabla \cdot (\nabla \times \underline{\mathbf{u}}) = 0 \tag{2.26}$$

On a side note, a flow with $\underline{\boldsymbol{\omega}} = 0$ is referred to as *irrotational* flow.

Shear strain can be thought of as the average decrease of the angle between two lines which are initially perpendicular to each other. Considering the lines $\overline{AB}$ and $\overline{BC}$ in Figure 2.2 as initial lines, the shear strain increment is $\frac{1}{2}(\mathrm{d}\alpha + \mathrm{d}\beta)$. Thus, making use of eqn (2.21), the shear strain rate is

$$\epsilon_{xy} = \frac{1}{2}\left(\frac{\mathrm{d}\alpha}{\mathrm{d}t} + \frac{\mathrm{d}\beta}{\mathrm{d}t}\right) = \frac{1}{2}\left(\frac{\partial v}{\partial x} + \frac{\partial u}{\partial y}\right) \tag{2.27}$$

Similarly,

$$\epsilon_{yz} = \frac{1}{2}\left(\frac{\partial w}{\partial y} + \frac{\partial v}{\partial z}\right) \qquad \epsilon_{zx} = \frac{1}{2}\left(\frac{\partial u}{\partial z} + \frac{\partial w}{\partial x}\right) \tag{2.28}$$

Note that shear strain rates are symmetric, i.e. $\epsilon_{ij} = \epsilon_{ji}$.

Finally, it remains to analytically define extensional strain (dilatation). Once again examining Figure 2.2, the extensional strain in direction of x is defined as the fractional increase in length of the horizontal side of the fluid element, given by

$$\epsilon_{xx}\mathrm{d}t = \frac{\left(\mathrm{d}x + \dfrac{\partial u}{\partial x}\mathrm{d}x\mathrm{d}t\right) - \mathrm{d}x}{\mathrm{d}x} = \frac{\partial u}{\partial x}\mathrm{d}t \tag{2.29}$$

with similar expressions for $\epsilon_{yy}\mathrm{d}t$ and $\epsilon_{zz}\mathrm{d}t$. Hence, the three dilatation strain rates are given by

$$\epsilon_{xx} = \frac{\partial u}{\partial x} \qquad \epsilon_{yy} = \frac{\partial v}{\partial y} \qquad \epsilon_{zz} = \frac{\partial w}{\partial z}. \tag{2.30}$$

These rates of strain form a second-order symmetric tensor

$$\underline{\underline{\boldsymbol{\epsilon}}} = \begin{pmatrix} \epsilon_{xx} & \epsilon_{xy} & \epsilon_{xz} \\ \epsilon_{yx} & \epsilon_{yy} & \epsilon_{yz} \\ \epsilon_{zx} & \epsilon_{zy} & \epsilon_{zz} \end{pmatrix}, \tag{2.31}$$

which will be shown to play a vital role in the derivation of the equation of motion.

2.4 Deformation law for a Newtonian fluid

In 1845, Sir George Gabriel Stokes postulated three assumptions which are valid for gases and most common fluids:

1. The fluid is continuous and its stress tensor σ_{ij} is at most a linear function of rates of strain ($\sigma_{ij} = f\left(\underline{\underline{\boldsymbol{\epsilon}}}\right)$).
2. The fluid is isotropic, i.e. its properties are independent of direction and therefore the deformation law is independent of the coordinate axes in which it is expressed.
3. When the strain rates are zero, the deformation law must reduce to the hydrostatic pressure condition $\sigma_{ij} = -p\delta_{ij}$.

The previous section shows that the tensor $\underline{\underline{\boldsymbol{\epsilon}}}$ is in fact symmetric, i.e. $\epsilon_{ij} = \epsilon_{ji}$. A property of symmetric tensors is that there exists one and only one set of axes for which the off-diagonal terms are zero. These are designated the *principal axes*, for which the strain rate tensor becomes

$$\underline{\underline{\boldsymbol{\epsilon}}}' = \begin{pmatrix} \epsilon'_{xx} & 0 & 0 \\ 0 & \epsilon'_{yy} & 0 \\ 0 & 0 & \epsilon'_{zz} \end{pmatrix}. \tag{2.32}$$

Condition 2 requires the principal strain axes be identical to the principal stress axes, which makes this a good basis from which to derive the deformation law. Let $\hat{\mathbf{x}}'$, $\hat{\mathbf{y}}'$, and $\hat{\mathbf{z}}'$ be the principal axes for which shear strain rates and shear stresses, i.e. the off-diagonal elements, are zero. Using these axes the deformation law can include at most three linear coefficients, for example

$$\sigma'_{xx} = -p + C_1\epsilon'_{xx} + C_2\epsilon'_{yy} + C_3\epsilon'_{zz}. \tag{2.33}$$

Note that $-p$ is added to satisfy condition 3. The condition of isotropy (condition 2) requires that $C_2 = C_3$, reducing the number of independent linear coefficients from three to two. Hence,

$$\sigma'_{xx} = -p + K\epsilon'_{xx} + C_2\left(\epsilon'_{xx} + \epsilon'_{yy} + \epsilon'_{zz}\right) = -p + K\epsilon'_{xx} + C_2\nabla\cdot\underline{\mathbf{u}}, \tag{2.34}$$

where $K = C_1 - C_2$, and the expression inside parentheses is the divergence of velocity. Eqn (2.34) may now be transformed to some arbitrary set of axes $\hat{\mathbf{x}}, \hat{\mathbf{y}}, \hat{\mathbf{z}}$ in which shear stresses are not equal to zero. Using directional cosines

$$\begin{array}{lll} \alpha_1 \equiv \hat{\mathbf{x}}'\cdot\hat{\mathbf{x}} & \beta_1 \equiv \hat{\mathbf{y}}'\cdot\hat{\mathbf{x}} & \gamma_1 \equiv \hat{\mathbf{z}}'\cdot\hat{\mathbf{x}} \\ \alpha_2 \equiv \hat{\mathbf{x}}'\cdot\hat{\mathbf{y}} & \beta_2 \equiv \hat{\mathbf{y}}'\cdot\hat{\mathbf{y}} & \gamma_2 \equiv \hat{\mathbf{z}}'\cdot\hat{\mathbf{y}} \\ \alpha_3 \equiv \hat{\mathbf{x}}'\cdot\hat{\mathbf{z}} & \beta_3 \equiv \hat{\mathbf{y}}'\cdot\hat{\mathbf{z}} & \gamma_3 \equiv \hat{\mathbf{z}}'\cdot\hat{\mathbf{z}} \end{array}$$

coordinates may be transformed from the arbitrary coordinate system to the principal coordinate system:

$$\hat{\mathbf{x}}' = \alpha_1\hat{\mathbf{x}} + \alpha_2\hat{\mathbf{y}} + \alpha_3\hat{\mathbf{z}}$$
$$\hat{\mathbf{y}}' = \beta_1\hat{\mathbf{x}} + \beta_2\hat{\mathbf{y}} + \beta_3\hat{\mathbf{z}}$$
$$\hat{\mathbf{z}}' = \gamma_1\hat{\mathbf{x}} + \gamma_2\hat{\mathbf{y}} + \gamma_3\hat{\mathbf{z}}$$

and vice-versa:

$$\hat{\mathbf{x}} = \alpha_1\hat{\mathbf{x}}' + \beta_1\hat{\mathbf{y}}' + \gamma_1\hat{\mathbf{z}}'$$
$$\hat{\mathbf{y}} = \alpha_2\hat{\mathbf{x}}' + \beta_2\hat{\mathbf{y}}' + \gamma_2\hat{\mathbf{z}}'$$
$$\hat{\mathbf{z}} = \alpha_3\hat{\mathbf{x}}' + \beta_3\hat{\mathbf{y}}' + \gamma_3\hat{\mathbf{z}}'.$$

By orthogonality of the coordinate system, it must hold that

$$\hat{\mathbf{x}}\cdot\hat{\mathbf{x}} = \hat{\mathbf{y}}\cdot\hat{\mathbf{y}} = \hat{\mathbf{z}}\cdot\hat{\mathbf{z}} = 1$$
$$\hat{\mathbf{x}}\cdot\hat{\mathbf{y}} = \hat{\mathbf{y}}\cdot\hat{\mathbf{z}} = \hat{\mathbf{z}}\cdot\hat{\mathbf{x}} = 0,$$

giving the identity

$$\alpha_l\alpha_m + \beta_l\beta_m + \gamma_l\gamma_m = \delta_{lm},$$

where δ_{lm} is the Kronecker delta. These definitions allow the following transformation rule for normal strain rates and stresses between the principal axes and the new arbitrary system:

$$\epsilon_{xx} = \epsilon'_{xx}\alpha_1^2 + \epsilon'_{yy}\beta_1^2 + \epsilon'_{zz}\gamma_1^2 \tag{2.35}$$
$$\sigma_{xx} = \sigma'_{xx}\alpha_1^2 + \sigma'_{yy}\beta_1^2 + \sigma'_{zz}\gamma_1^2 \tag{2.36}$$

Similarly, shear strain and stress can be expressed in terms of principal strain rates and stresses:

$$\epsilon_{xy} = \epsilon'_{xx}\alpha_1\alpha_2 + \epsilon'_{yy}\beta_1\beta_2 + \epsilon'_{zz}\gamma_1\gamma_2 \tag{2.37}$$
$$\sigma_{xy} = \sigma'_{xx}\alpha_1\alpha_2 + \sigma'_{yy}\beta_1\beta_2 + \sigma'_{zz}\gamma_1\gamma_2 \tag{2.38}$$

Now to eliminate σ'_{xx}, σ'_{yy}, and σ'_{zz} from eqn (2.36) by using eqn (2.34) in conjunction with eqn (2.35) and the fact that $\alpha_1^2 + \beta_1^2 + \gamma_1^2 = 1$:

$$\sigma_{xx} = -p + K\epsilon_{xx} + C_2\nabla\cdot\underline{\mathbf{u}}. \tag{2.39}$$

Similar expressions can be obtained for σ_{yy} and σ_{zz}. Also, σ'_{xx}, σ'_{yy}, and σ'_{zz} may be eliminated from eqn (2.38), resulting in

$$\sigma_{xy} = K\epsilon_{xy} \tag{2.40}$$

with analogous expressions for σ_{yz} and σ_{xz}. Note how the symmetry of ϵ_{ij} translates to σ_{ij}. For Newtonian fluids, K is typically equal to 2μ, twice the *ordinary coefficient*

of viscosity (usually called the *dynamic viscosity*, or simply the *viscosity*), and C_2, the *second coefficient of viscosity*, is usually referred to as the *coefficient of bulk viscosity* λ, as it is associated with volume expansion ($\nabla \cdot \underline{\mathbf{u}}$). Combining eqn (2.39) and eqn (2.40) yields a general deformation law for Newtonian viscous fluids:

$$\sigma_{ij} = -p\delta_{ij} + \mu\left(\frac{\partial u_i}{\partial x_j} + \frac{\partial u_j}{\partial x_i}\right) + \lambda\nabla \cdot \underline{\mathbf{u}}\delta_{ij}, \tag{2.41}$$

where the rates of strain ϵ_{ij} are now presented in terms of velocity gradients.

2.5 Mechanical and thermodynamic pressure

A direct consequence of eqn (2.41) was pointed out by Stokes in that he defined the mechanical pressure p_M as the average compression stress exerted on a control volume equal to $-\frac{1}{3}tr\left(\underline{\boldsymbol{\sigma}}\right)$, which may also be expressed using (2.41). Hence,

$$p_M = -\frac{1}{3}\left(\sigma_{xx} + \sigma_{yy} + \sigma_{zz}\right) = p - \left(\frac{2}{3}\mu + \lambda\right)\nabla \cdot \underline{\mathbf{u}}. \tag{2.42}$$

This means that the average pressure in a viscous fluid under stress is not the same as the thermodynamic property called pressure. p_M also takes volume expansion into account, which exerts a force opposite to p. Stokes circumvented this problem in 1845 by assuming

$$\mu = -\frac{2}{3}\lambda \tag{2.43}$$

which is known as *Stokes' hypothesis*. Also, in incompressible fluids this problem vanishes as constant density implies $\nabla \cdot \underline{\mathbf{u}} = 0$. This is discussed later in Section 2.10.